MTL TR 92-49 **AD-A255 593** AD

USE OF THE THIN-WALLED TORSION SPECIMEN

CHARLES S. WHITE
MATERIALS DYNAMICS BRANCH

DTIC
ELECTE
SEP 15 1992
S A D

August 1992

92 9 14 070

92-25174

39F58D

29 pgp

The findings in this report are not to be construed as an official Department of the Army position, unless so designated by other authorized documents.

Mention of any trade names or manufacturers in this report shall not be construed as advertising nor as an official indorsement or approval of such products or companies by the United States Government.

DISPOSITION INSTRUCTIONS

Destroy this report when it is no longer needed.
Do not return it to the originator

REPORT DOCUMENTATION PAGE		READ INSTRUCTIONS BEFORE COMPLETING FORM
1 REPORT NUMBER MTL TR 92-49	2. GOVT ACCESSION NO.	3. RECIPIENT'S CATALOG NUMBER
4. TITLE (and Subtitle) USE OF THE THIN-WALLED TORSION SPECIMEN		5. TYPE OF REPORT & PERIOD COVERED Final Report
		6 PERFORMING ORG. REPORT NUMBER
7. AUTHOR(s) Charles S. White		8. CONTRACT OR GRANT NUMBER(s)
9. PERFORMING ORGANIZATION NAME AND ADDRESS U.S. Army Materials Technology Laboratory Watertown, Massachusetts 02172-0001 SLCMT-MRD		10. PROGRAM ELEMENT. PROJECT, TASK AREA & WORK UNIT NUMBERS AMCMS: 612105.H840011
11 CONTROLLING OFFICE NAME AND ADDRESS U.S. Army Laboratory Command 2800 Powder Mill Road Adelphi, MD 20783-1145		12. REPORT DATE August 1992
		13. NUMBER OF PAGES 24
14. MONITORING AGENCY NAME & ADDRESS(if different from Controlling Office)		15. SECURITY CLASS. (of this report) Unclassified
		15a. DECLASSIFICATION/DOWNGRADING SCHEDULE

16. DISTRIBUTION STATEMENT (of this Report)

Approved for public release; distribution unlimited.

17. DISTRIBUTION STATEMENT (of the abstract entered in Block 20, if different from Report)

18. SUPPLEMENTARY NOTES

19. KEY WORDS (Continue on reverse side if necessary and identify by block number)

Metal plasticity   Torsion
Finite element analysis
Deformation

20. ABSTRACT (Continue on reverse side if necessary and identify by block number)

(SEE REVERSE SIDE)

DD $_{1\ JAN\ 73}^{FORM}$ 1473   EDITION OF 1 NOV 65 IS OBSOLETE

Block No. 20

ABSTRACT

The thin-walled torsion specimen has been analyzed by the finite element method to determine its usefulness in material testing. A particular geometry, having a short gauge section and thick shoulder regions, was examined using material constants for 316 stainless steel. The specimen was analyzed with an eye toward determining its usefulness in approximating simple shear deformation. Both forward and single reverse behavior were examined.

Classical isotropic and Prager-Ziegler kinematic hardening (using Jaumann stress rates) were used in the analyses. The gauge section did not contain uniform stress components throughout, but nevertheless, the macroscopic response of the specimen compared favorably with simple shear results. Plastic deformation was not entirely constrained to the gauge section but it extended some distance into the shoulder region. Consequently, the shear strain in the gauge section must be directly measured with an extensometer or a correction factor used when converting the applied machine rotation to gauge shear strain. This correction factor was determined from the finite element calculations. In reverse twisting, the macroscopic response of the specimen again matched well with simple shear results but neither material law provided even a qualitative match with experiment. The limitations of the thin-wall specimen are described and quantified in this report.

CONTENTS

INTRODUCTION

Determining the behavior of materials, particularly metals, to large deformation conditions has presented substantial experimental difficulties from the time of Tresca's early metalworking experiments to the present. Primary difficulties have been in determining the stress and strain accurately in an experimental test specimen that undergoes gross deformation. A homogeneous test region is required which is free from large stress or strain gradients and is large enough to measure displacements from which strain can be inferred. Tension, compression, rolling, extrusion, torsion and drawing are all types of procedures that have been applied to metals to achieve large deformation. Comprehensive reviews of large deformation experiments are available.[1, 2]

The thin-walled torsion specimen has received considerable attention in the literature in recent years because it offers the possibility of a simple deformation field and homogeneous stress and strain states. A specimen which has a wall which is only a small fraction of the radius of the section will have a nearly uniform strain distribution through the wall thickness. The nominal stress state is given by dividing the required torque or axial (thrust) load by the cross sectional area and mean radius. The specimen is known to be unstable at large strains when it is proportioned by conventional means having long uniform gauge sections with gradual transition to the gripping region. Torsional buckling is a primary mode of failure for such a specimen. This problem can be suppressed by shortening the gauge length so that it is only a fraction of the diameter of the gauge section. A specimen of this type was first proposed by Hodierne[3] for use in hot working studies and popularized by Lindholm et al.[4] Figure 1 shows a generic sketch of this type of specimen. Notice the short, thin-walled gauge section which quickly transitions to the thick-walled shoulder region where the specimen is gripped. Table 1 lists some of the researchers who have used this type of specimen for large strain testing. Also shown are two important geometric ratios: the gauge length divided by the average diameter of the wall region, and the average diameter divided by the wall thickness. The larger these ratios are, the more likely buckling is to occur. This presents a trade off in specimen design since a larger diameter/wall thickness ratio gives a more uniform stress and strain through the wall.

Although originally used to compare normalized flow stress behavior with tension/compression results (Hecker), the torsion test offers the potential for discriminating material models as illustrated by

1. Gil Sevillano, J., Van Houtte, P., and Aernoudt, E., *Large Strain Work Hardening and Textures*, Progress in Materials Science volume 25, 1981, pp. 69-412.
2. Hecker, S.S., Stout, M.G., and Eash, D.T., *Experiments on Plastic Deformation at Finite Strains*, Plasticity of Metals at Finite Strain: Theory, Experiment and Computation, E.H. Lee and R.L. Mallett, eds., Proceedings of Research Workshop held at Stanford University, June 29 - July 1, 1981, pp. 162-205.
3. Hodierne, F.A., *A Torsion Test for Use in Metalworking Studies*, Journal of the Institute of Metals, Vol. 91, 1962, pp. 267-273.
4. Lindholm U.S., Nagy, A., Johnson, G.R., and Hoegfeldt, J.M., *Large Strain, High Strain Rate Testing of Copper*, ASME Journal of Engineering Materials and Technology, Vol. 102, 1980, pp. 376-381.

Table 1. Geometry of Torsion Specimens Used in the Literature

Researcher	Gauge Length/Diameter	Diameter/Wall Thickness
Hodierne[3] (1962)	0.40	5.
Bailey, Haas, Nawab[5] (1972)	0.42	6.
Eleiche and Campbell[6] (1976)	0.08	43.
Senseny, Duffy, Hawley[7] (1978)	0.16	29.-42.
Lindholm et al.[4] (1980)	0.23	16.4
Lipkin, Chiesa, Bammann[8] (1987)	0.24	15.7
White, Bronkhorst, Anand[9] (1990)	0.31	26.
Weerasooriya and Swanson[10] (1991)	0.30	27.
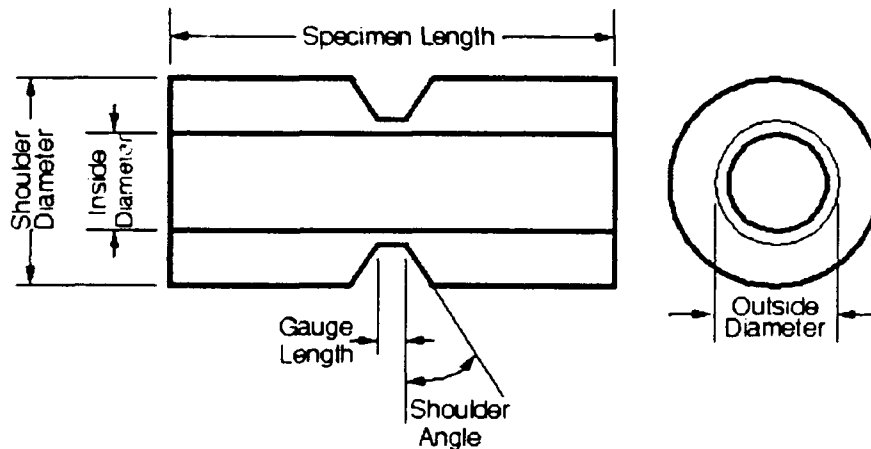
Figure 1. Geometry of the thin-walled torsion specimen.

5. Bailey, J.A., Haas, S.L., and Nawab, K.C., *Anisotropy in Plastic Torsion*, Journal of Basic Engineering, March 1972, pp. 231-237.

6. Eleiche, A.M., and Campbell, J.D., *Strain-rate Effects During Reverse Torsional Shear*, Experimental Mechanics, Vol. 16, 1976, pp. 281-290.

7. Senseny, P.E., Duffy, J., and Hawley, R.H., *Experiments on Strain Rate History and Temperature Effects During the Plastic Deformation of Close-Packed Metals*, ASME Journal of Applied Mechanics, Vol. 45, 1978, pp. 60-66.

8. Lipkin, J., Chiesa, M.L., and Bammann, D.J., *Thermal Softening of 304L Stainle. s Steel: Experimental Results and Numerical Simulations*, Proceedings of IMPACT '87, Bremen, FRG, May 1987.

9. White, C.S., Bronkhorst, C.A., and Anand, L., *An Improved Isotropic-Kinematic Hardening Model for Moderate Deformation Metal Plasticity*, Mechanics of Materials, Vol. 10, 1990, pp. 127-147.

10. Weerasooriya, T., and Swanson, R.A., *Experimental Evaluation of the Taylor-Type Polycrystal Model for the Finite Deformation of an FCC Metal (OFHC Copper)*, U.S. Army Materials Technology Laboratory, MTL TR 91-20, 1991.

the simple shear predictions of Nagtegaal and deJong.[11] In the past decade there has been intensive work aimed at describing material behavior in large simple shear and even formulating constitutive models with the specific goal of describing simple shear in a more intuitively acceptable manner. In light of these results the torsion test has a new importance insofar as it provides an approximation to simple shear deformation.

The kinematics of the finite strain tension-torsion of a thin-walled tube have been examined in detail by McMeeking.[12] For a uniformly deforming tube, the stretching tensor (symmetric part of the velocity gradient) can be written in curvilinear coordinates as:

$$
D = \begin{bmatrix} \dfrac{\dot{t}}{t} & 0 & 0 \\[2mm] 0 & \dfrac{\dot{r}}{r} & \dfrac{\dot{\gamma}}{2} \\[2mm] 0 & \dfrac{\dot{\gamma}}{2} & \dot{\varepsilon} \end{bmatrix} \tag{1}
$$

Here the 1, 2, and 3 directions are in the radial, hoop and axial directions, respectively. The torsion test provides an approximation to simple shear only as well as it restrains the changes in wall thickness, t, mean radius, r, and axial strain , ε, to be zero. The geometry shown in Figure 1 attempts to enforce the gauge section to be free from normal stretches by the presence of the large shoulders near the gauge region. The massive shoulders prevent large radius change. The grips restrain axial motion to within the stiffness of the testing machine frame and the thick walls of the shoulder region transmit this axial stiffness to the gauge region. The effectiveness of the geometry of the torsion specimen to restrain the radial, hoop and axial straining in the testing of metals is one of the primary features to be determined in evaluating the torsion test.

The experimental programs referred to in Table 1 all use some form of the thin-walled specimen but not in a careful way for determining multiaxial stress response. The largest use is to determine just the shear stress response for finite twisting. This can be meaningful or not depending upon the restraint in the axial direction. For the torsion specimen to be able to approximate simple shear it must be able to ensure axial straining in the gauge section is very small. This requires both stiff testing machines and stiff grips. Measurement of the induced axial force required to prevent axial straining is desired in this type of test.

11. Nagtegaal, J.C., and de Jong, J.E., *Some Aspects of Non-Isotropic Workhardening in Finite Strain Plasticity, Plasticity of Metals at Finite Strain: Theory, Experiment and Computation*, E.H. Lee and R.L. Mallett, eds., Proceedings of Research Workshop held at Stanford University, June 29 - July 1, 1981, pp. 55-101.

12. McMeeking, R.M., *The Finite Strain Tension Torsion Test of a Thin-Walled Tube of Elastic-Plastic Material*, International Journal of Solids and Structures, Vol. 18, 1982, pp. 199-204.

The first experimental results which presented measured axial stresses from thin-walled tubular tests were from White and Anand in 1986 for 1100 aluminum (see Aifantis[13]) and Lipkin et al.[8] for 304L stainless steel. Since these first tests only a small number of others have been reported. White et al.[9] give the shear and axial normal stress histories for monotonic twisting of 316 stainless steel, 1100 aluminum, and three carbon steels 1020, 1045, and 1095. Weerasooriya and Swanson[10] presented similar results for the finite twisting of polycrystalline copper. In all of the above reported tests the specimens were twisted to a final shear strain between 0.9 and 5. The shear stresses invariably increased monotonically with deformation. The axial normal stresses were compressive and increased monotonically in magnitude for all of the materials except for copper. It had a compressive maximum then reversed and even became tensile.

Lipkin and Lowe[14] presented the interesting result for the reverse twisting of a specimen of 304L stainless steel. The shear stress exhibits the same behavior as the tension/compression reverse straining behavior would be expected to show (with the anomolous inflection as the stress passes through zero, probably due to the method of gripping the specimen with pins). The axial stress magnitude quickly recovered toward zero as reverse twisting commenced but then passed through a nonzero minimum and gradually increased back toward the value it had prior to unloading. This behavior is very interesting. It is similar to the multiaxial ratchetting seen in a variety of studies[15] where, for instance, a tube is twisted back and forth in a cyclical torsional manner. A transient in the length change is seen where the specimen initially shortens but then lengthens during each half-cycle. Lowe and Lipkin[16] have used a polycrystal plasticity model to examine the simple approximation to their reverse experiment. They showed correct prediction of some of the qualitative features of the axial strain transient. They noted that these results were sensitive to the amount of axial restraint applied to the calculation. The axial stiffness of the testing machine and shoulder region could have an important bearing on the material response.

PREVIOUS ANALYSES

The thin-walled torsion specimen has been used largely without investigation, either experimentally or numerically as to its effectiveness in simulating simple shear. The two exceptions are Johnson[17] and Lipkin, Chiesa and Bammann.[8] Johnson[17] conducted a two-dimensional analysis of the test specimen using the EPIC-2 lagrangian, finite element hydrocode. The analysis included both heat conduction/generation and strain rate effects. These results present no information about the stress and strain distributions in the test specimen but rather were concerned with matching a viscoplastic constitutive law to

13. Aifantis, E.C., *The Physics of Plastic Deformation*, International Journal of Plasticity, Vol. 3, 1987, pp. 211-247.
14. Lipkin, J., and Lowe, T.C., Proceedings of Plasticity '89, The Second International Symposium on Plasticity and its Current Applications, August 1989, Tsu, Japan.
15. Freudenthal, A.M., and Ronay, M., *Accumulation of Second-Order Strain in Workhardening Media*, IUTAM Symposium, June 1966, Springer-Verlag, New York.
16. Lowe, T.C., and Lipkin, J., *Analysis of Axial Deformation Response During Reverse Shear*, submitted to the Journal of the Mechanics and Physics of Solids, 1991.
17. Johnson, G.R., *Dynamic Analysis of a Torsion Test Specimen Including Heat Conduction and Plastic Flow*, ASME Journal of Engineering Materials and Technology, Vol. 103, 1981, pp. 201-206.

macroscopic experimental results (Lindholm et al.[4]). This analysis does not address the question of how well the thin-walled specimen simulates simple shear. It is of note that Johnson did observe that not all of the plastic deformation occurs in the thin test section. For very large shear strains he noted that only 87 percent of the specimen rotation occurs in the test section.

Lipkin et al.[8] presented more detailed numerical results of their test specimen using the DYNA3D finite element hydrocode. The analysis was conducted for the express purpose of comparing experimental results of the authors with their particular constitutive model. As such, no comparison was made with better understood, more classical material models. This limits the usefulness of their analysis for general evaluation of the specimen but a number of excellent observations were made. The gauge length shows a slight lengthening during torsion even for perfectly fixed specimen ends. This lengthening was both measured experimentally and simulated numerically. The shear strain at an element in the gauge section was shown to differ from the average shear strain calculated from the twist of the grips. The shear strain was quite uniform in the gauge section below shear strains of about 200% but as twisting was continued above this level the shear strain distribution varied considerably. This variation was in such a way as to suggest axial buckling was occurring.

There are two main limitations to Lipkin et al.[8] analysis. First, classical plasticity laws were not used to allow easy understanding of whether the macroscopic numerical results yielded results consistent with the predictions of simple shear. Second, the finite element mesh that was used was very coarse containing only 3 elements through the thickness. The elements they used were eight node brick type elements with reduced integration. This left only three material integration points through the thickness of the specimen wall. Also, no mesh convergence comparisons were reported.

The results of Lipkin et al.[8] have shed new light on the behavior of the thin-walled torsion specimen but have not provided a detailed, quantitative assessment as to the limitations and usefulness of the specimen. The current analysis addresses these questions.

FINITE ELEMENT MODEL

The specimen geometry that was simulated corresponds to the 316 stainless steel specimen reported in White et al.[9] (See Figure 1). The gauge length was 5.9 mm. The inside diameter was 19.05 mm. The outside diameter of the gauge region was 20.52 mm. The outside diameter of the shoulder region was 38.1 mm and the shoulder angle was 30 degrees.

The finite element analysis was conducted with the ABAQUS[18] finite element program. All of the elements were eight node, linear displacement bricks having a full eight material integration points (C3D8 elements in ABAQUS).

---

18. ABAQUS Users Manual, 1989, Hibbiu Karlsson and Sorenson, Inc., Providence, RI.

5

The mesh, shown in Figure 2, discretized the specimen into just one circumferential slice of either one or five degree extent. A fine mesh within that slice was used. Each slice had 9 elements through the wall thickness and 15 along the axial length of the one-half gauge length. Again, the nodes on the midplane of the gauge region were restrained against both axial and circumferential motion but radial motion was allowed. The nodes along the top face of the shoulder region were restrained against axial motion. The outer node on the top face was constrained to move in a circular arc simulating the applied twist. The compatibility enforced on this strip to make it simulate an entire circumference was by re-quiring the corresponding nodes on the two faces of the strip to retain the prescribed circumferential an-gle (either one or five degrees) between them.   This required displacement relation between two equiva-lent nodes on opposite faces of the slice are given by Equation 2.

$$
\begin{bmatrix} {}^{B}u^{j}_{x} \\ {}^{B}u^{j}_{y} \\ {}^{B}u^{j}_{z} \end{bmatrix} = \begin{bmatrix} \cos\theta & -\sin\theta & 0 \\ \sin\theta & \cos\theta & 0 \\ 0 & 0 & 1 \end{bmatrix} \begin{bmatrix} {}^{A}u^{j}_{x} \\ {}^{A}u^{j}_{y} \\ {}^{A}u^{j}_{z} \end{bmatrix} \tag{2}
$$

Here θ is the prescribed angle between faces A and B and ${}^{B}u^{j}_{x}$ is the global displacement in the x direction of the jth node of the B face.

A complete circumferential mesh was used for comparison with the single slice model. It had a coarse discretization with only 7 elements through the wall thickness and 18 elements around the cir-cumference.
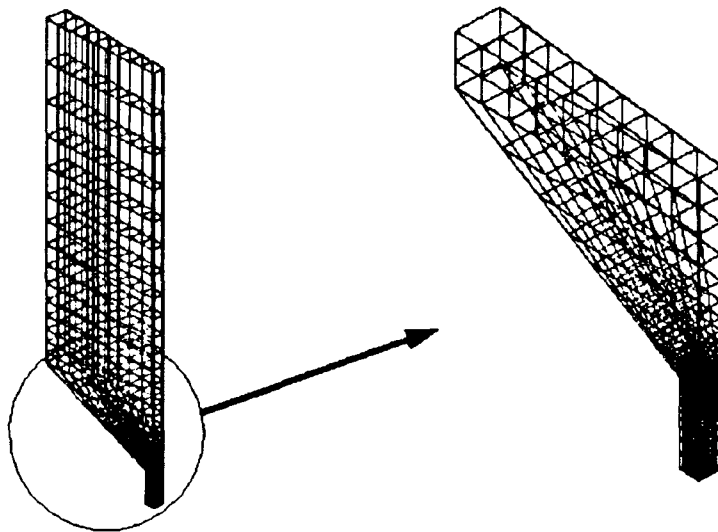

Figure 2. Finite element mesh used to simulate the torsion specimen.

The material models that were used in the simulations were classical, large strain plasticity laws: isotropic hardening, kinematic hardening, and perfect plasticity. These were chosen since their behavior under simple shearing deformation is well known (Nagtegaal and deJong[11]). The Jaumann stress rate was used. It is widely recognized that choice of the stress rate can greatly affect axial stress in simple shear (Dafalias,[19] Reed and Atluri,[20] Aifantis[13]). Finite element anaiyses using all of the proposed rates are beyond the scope of this paper. For simple shearing type deformation, the Jaumann rate with classical isotropic and kinematic hardening bound the behavior both of experimental results and of most of the constitutive laws in the literature. For elastic properties, a Young's modulus of 200 GPa and Poisson's ratio of 0.33 were used. The material had an initial yield stress of 250 MPa and a constant plastic hardening modulus of 1500 MPa. Convergence studies were conducted of the time step size and nodal force tolerance in the acceptance criterion for the finite element studies. The automatic load stepping was used in full large deformation analysis. Approximately 100 displacement increments were used to twist the specimen to a nominal engineering shear strain of unity.

FINITE ELEMENT RESULTS FOR FORWARD TWISTING

The majority of the comparisons of the numerical results are shown in terms of macroscopic variables that would be determined in an experiment. The nominal shear stress in the gauge section was determined by taking the torque from summing the circumferential reaction forces on the top face of the specimen and dividing by the cross sectional area and average radius of the gauge section. The axial normal stress was determined in similar manner by summing the axial reaction force on the top face of the specimen and dividing by the gauge cross sectional area. The average strains in the gauge section were determined assuming an extensometer could measure the circumferential and axial displacements on the outside of the gauge section at the intersection with the transition region to the shoulder. The nominal axial strain was determined by dividing the axial displacement by the original gauge length and the nominal average shear strain (engineering) by dividing the arc displacement by the original gauge length. These numerical results then can be compared with the variables measured in an experimental test.

The different models described above were compared for calculations using both isotropic and kinematic hardening. The macroscopic stress-strain results and the stress and strain contours within the specimen were virtually identical. The models: full circumferential, one degree slice and five degree slice all yielded results that were almost indistinguishable. This was taken as verification that the mesh was sufficiently fine and the boundary conditions for the single slice meshes were appropriate. Most of the succeeding results that will be discussed were obtained with the single slice model having five degrees circumferentially.

19. Dafalias, Y.F., *A Missing Link in the Formulation and Numerical Implementation of Finite-Transformation Elastoplasticity*, Constitutive Equations: Macro and Computational Aspects, William, K.J., ed., ASME, 1994, pp. 25-40..
20. Reed, K.W., and Atluri, S.N., *Constitutive Modeling and Computational Implementation in Finite Strain Plasticity*, International Journal of Plasticity, Vol. 1, 1985, pp. 63-87.
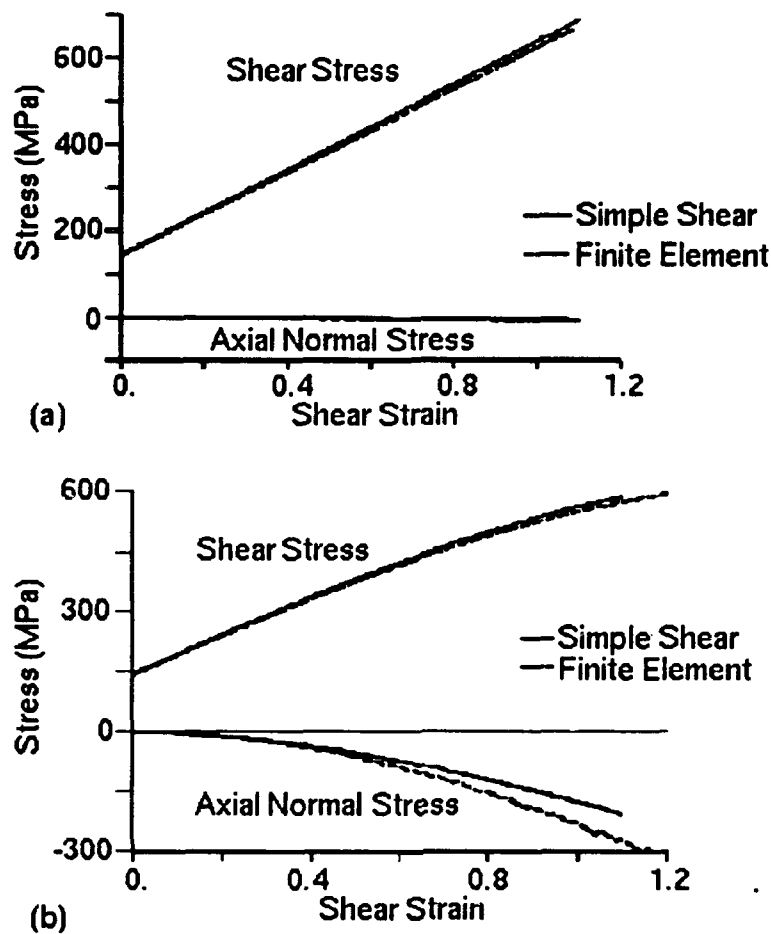
Figure 3. Comparison of finite element simulation with simple
shear for isotropic hardening (a) and kinematic hardening (b).

In order to evaluate how well the thin-walled torsion specimen approximates simple shear a compar-
ison is made between the shear and normal stress response inferred from the finite element simulation
with that for the same constitutive models integrated directly assuming only simple shear deformation.
The results of this comparison are shown in Figure 3 for both isotropic and kinematic hardening. For
isotropic hardening we see an almost exact correlation. No normal stress develops and the shear stress
linearly increases with strain. For kinematic hardening (using Jaumann derivatives) a substantial axial
normal stress is predicted both by the finite element model of the specimen and the assumed simple
shear deformation. The finite element model predicts an axial normal stress approximately 20% larger
than produced by simple shear. Notice that the shear stress is quite well correlated by the specimen and
simple shear.

The distribution of various Cauchy stress components is shown in Figure 4 for kinematic hardening
at a nominal engineering shear strain in the gauge section of 91%. Figure 4a shows the cross section of

8

the near gauge length region as well as the two radial lines, A and B, that were used to plot the distributions of stress components shown in Figure 4b. The solid curves in Figure 4b correspond to cross sectional line A. Notice that the shear stress is quite uniform across the wall thickness but the hoop and axial normal stresses have a large variation. This is a result of the center of the specimen pulling in due to the tensile hoop stress. For simple shear, the hoop stress should be equal in magnitude and opposite in sign to the axial stress. This can not be maintained for a long thin-walled tubular specimen. The diameter of the center of the gauge section decreases slowly as the specimen is deformed. The diametral decrease for the configuration shown in Figure 4a is 0.8%. This is not enough of a change to dramatically alter the geometry and would not be considered a buckle. It does create a superimposed bending type of stress gradient through the wall thickness at this location.

The dashed curves show that at location B the stresses are much more uniform across the wall thickness. The variations in both the hoop and axial stresses along line B are about 16%. At this location the stress response of simple shear is maintained quite well.

The reason for the increased axial normal stress when compared to simple shear (Figure 3) can be traced to the slight diameter decrease away from the shoulders and the fact that the plastic deformation is not completely contained in the gauge section. Figure 5 shows the contours of equivalent plastic strain at a grip rotation of 0.3 rad. Notice that the contour of 0.1% plastic strain extends into the transition region for more than one-half gauge length. The plastic deformation is not constrained to the gauge section. This has two effects on the kinematics. The first is that the axial restraint is not perfect.

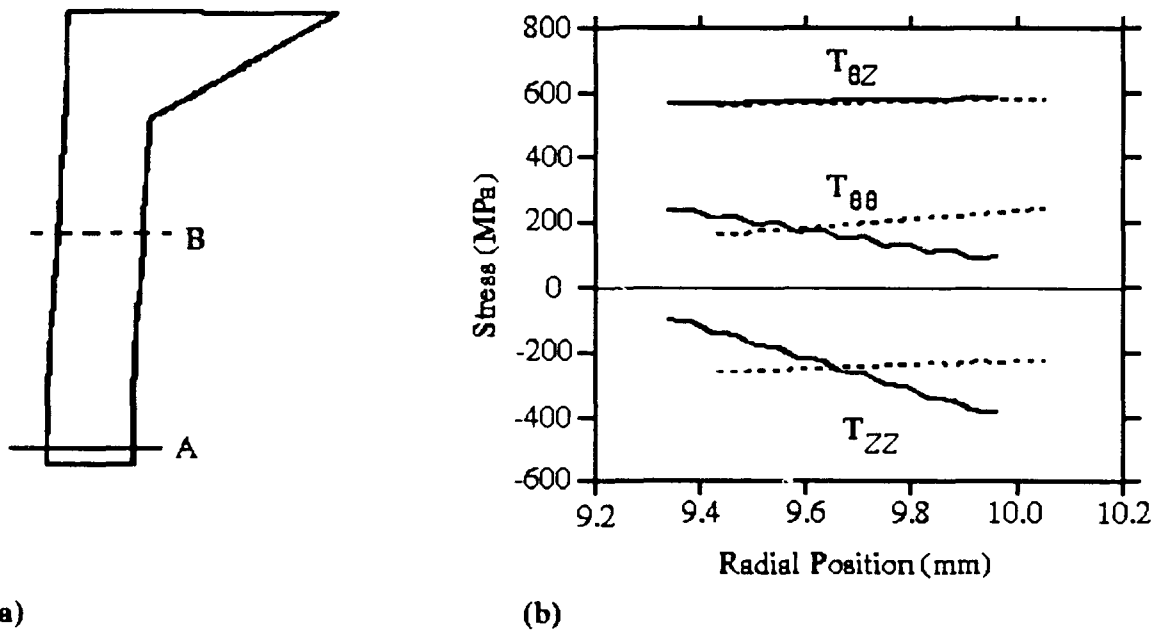
(a)   (b)

Figure 4. Variation of stress components with radial position across the thickness at two locations in the gauge. (a) Deformed specimen geometry and location for stress distributions. (b) Variation of stress components along line A (solid curves) and line B (dashed curves).

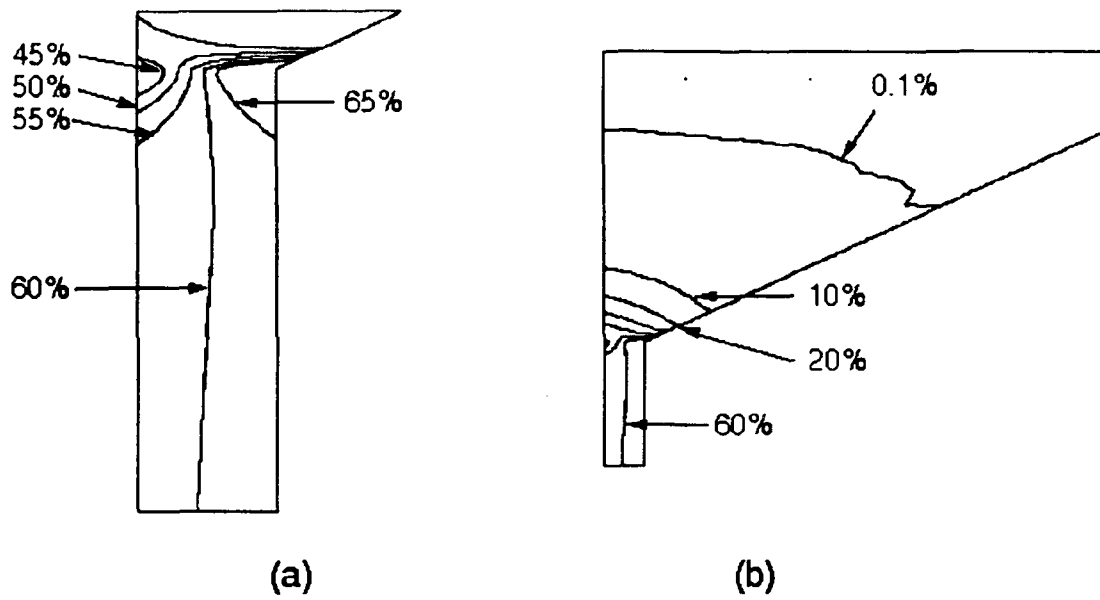**(a)**   **(b)**

Figure 5. Contours of equivalent plastic strain plotted on the original cross section.

Figure 6 shows the development of average axial strain across the gauge length with shear strain. For the three plasticity laws considered, an extension of the gauge length is observed during testing. The magnitude of this strain is small but it is enough to increase the axial stress, especially for kinematic hardening. For strict simple shear conditions in the gauge region, the axial strain would be zero. This small axial strain is coupled with the slight decrease in the radius at the center of the gauge section.
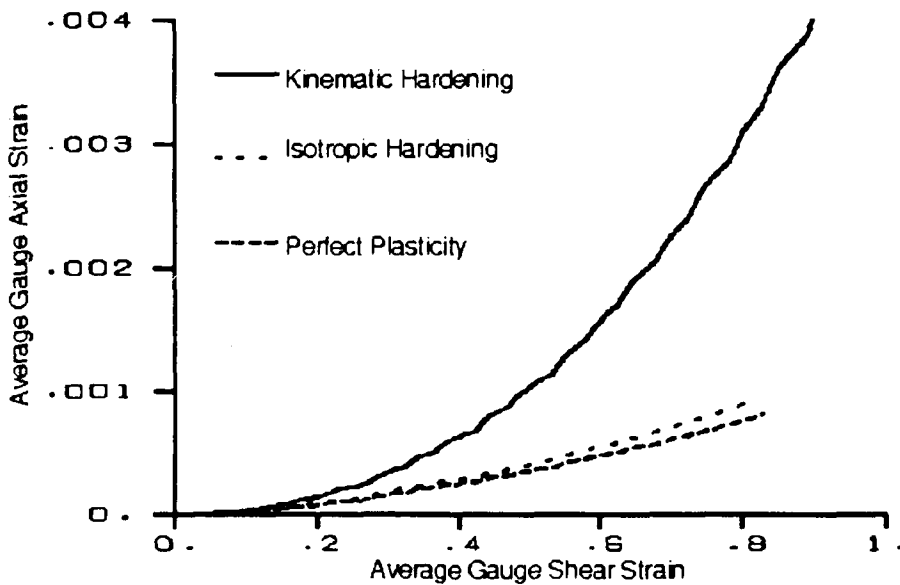
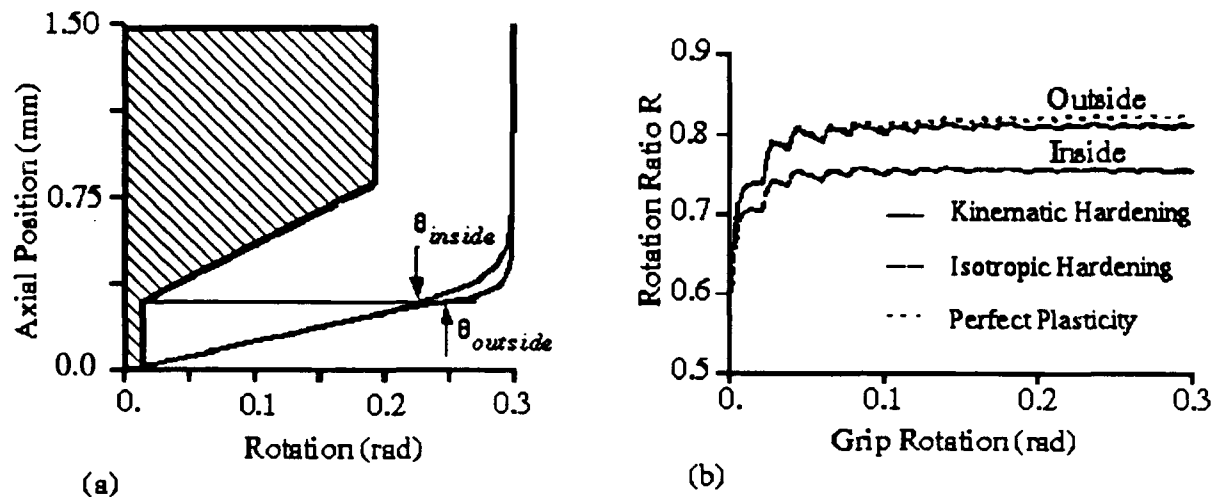Figure 6. Development of axial strain in the gauge section with deformation.

10

Figure 7. Ratio of rotation in the gauge section to total applied rotation. (a) Variation of rotation with axial position along inside and outside surfaces of the specimen. (b) Evolution of rotation ratio with applied rotation for various hardening laws.

Another effect of the plastic strain extending into the transition shoulder region is on the shear strain. In the results presented above, the shear strain was calculated by taking the twist calculated across the gauge section and converting to strain. In experimental practice, the twist applied by the testing machine has been assumed to be entirely transmitted into the gauge section and hence it has been used to calculate the shear strain. Figure 7a illustrates the way that the twist applied at the grips is distributed along the length of the specimen. Not all of the rotation is confined to the gauge section although the rotation does vary quite uniformly in the gauge section indicating uniform shear strain. The curves for both the inner surface and the outer surface of the specimen are shown. They are identical except right at the transition to the shoulder region. This would give slightly different values for rotational extensometers (Wu and Xu[21]) placed on the inner versus outer surface at this location. From the finite element results, we compare the twist measured across the gauge section with the twist applied across the entire specimen. In Figure 7b the ratio of these twists (R = $(\Delta\phi)$ gauge / $(\Delta\phi)$ total) is plotted against rotation for both the inner and outer surfaces. For the geometry considered here, the ratio is seen to be independent of hardening model. It is also independent of applied strain after an initial transient. The rotation ratio does depend slightly whether it is measured along the inner surface or the outer surface of the specimen. For this specimen, about 78% of the twist that is applied at the grips actually goes into the deformation in the gauge section. It is fortuitous that this ratio is independent of hardening model and deformation level. A simple correction factor can be applied to the experimentally measured twist in converting to shear strain (just multiply by 0.78). This correction factor is dependent

21. Wu, H.C., and Xu, Z., *An Axial-Torsional Extensometer for Finite Deformation*, ASME Journal of Engineering Materials and Technology, Vol. 112, 1990, pp. 330-335.

upon the particular specimen geometry and flow stress curve but can be easily evaluated from finite element modeling. Of course, experimentally one would like to have a rotational extensometer to measure the twist in the gauge section. This correction factor is the next suitable approach.

In order to try to limit the spread the of plasticity into the shoulder a simulation was considered where the shoulder made an abrupt transition to the gauge with a shoulder angle of zero degrees. In results not shown here this square cornered specimen behaved in essentially the same manner as the previous geometry. The macroscopic stress response was virtually identical to the results for the tapered shoulder. The plastic strain was still observed to extend the same way, as previously observed, into the shoulder region. The results do not seem sensitive to the angle of this transition. Note that this applies to the simulation with a moderate amount of strain hardening. The level of strain hardening will determine how well contained the plastic flow is to the gauge region. For a metal with little strain hardening, like high strength steel, the plastic deformation should extend very little distance into the shoulder. For a metal which exhibits a large amount of strain hardening, like annealed copper, the entire shoulder region could deform plastically if not designed correctly.

For the tapered shoulder geometry illustrated in Figure 1, the gauge length was varied to see what its affect would be on the axial stress/strain history. The geometry considered so far has a gauge length to wall thickness ratio of approximately 8 (g/t=8). Simulations were conducted where the gauge length ratio was varied from 8 to 1. In Figure 8 the macroscopic stress/strain results are shown for these simulations. The trend can be seen that as the gauge length is shortened both the shear stress and axial normal stress decrease in magnitude. For a ratio of 4 we can see that the simple shear results are matched very closely. This would be the optimal ratio for this design for this material. Unfortunately, the analytical
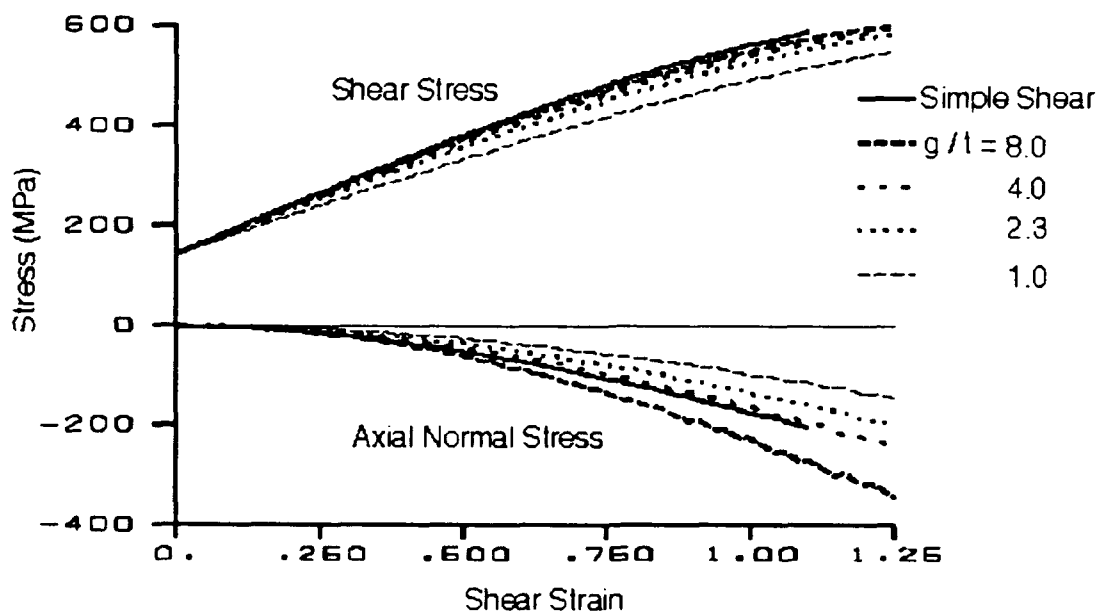

Figure 8. Effect of gauge length on the stress response to kinematic hardening.

12

simple shear results are not matched for shorter gauge lengths than this optimal value. The usefulness of the type of analysis shown here is clearly seen. The finite element modeling allows us to choose the best parameters for the specimen.

SUMMARY OF FORWARD LOADING RESULTS

In the preceding sections the thin-walled specimen was analyzed for unidirectional twisting. The main results can be summarized as follows. Results were presented for the stress strain distribution in the gauge region and the macroscopic response of the specimen. Even though the stresses were not uniform throughout the gauge section the macroscopic response of the specimen was close to that which would be predicted assuming simple shear deformation. This good correspondance was attributed to the existence of a cross section in the gauge region where the stresses were uniform and the simple shear solution did hold. The calculations also showed that not all of the twist that was applied to the shoulder region of the specimen was transmitted to the gauge region. Plastic deformation extended from the gauge into the transition region to the shoulder. A factor was defined and calculated which should be multiplied by the applied twist in converting the experimental torque/twist curve to stress/shear strain. This factor was constant over all of the larger deformation and independent of material model within the limits bounded by classical isotropic/kinematic hardening. This allows the shear strain to be calculated correctly when a torsional extensometer is not available.

REVERSE TORSION TESTING

The thin-walled torsion specimen is also examined as a test specimen for conducting reverse straining experiments. Deformation is conducted in one direction, then reversed to bring the specimen back to its original configuration.

The use of the thin-walled specimen for reverse shear was shown by Lipkin and Lowe[14] in 1989 for 304L stainless steel. They twisted their specimen to an engineering shear strain of about 160% then reversed the twist back to a total strain approaching zero. There was an anomaly in their shear stress response during reverse because the specimen was gripped with a single cross pin. A very interesting axial stress response was seen nonetheless. During reverse, the compressive axial stress initially went toward zero very rapidly but then recovered and reached nearly the same magnitude that it had prior to reverse. This behavior was not expected since it is not predicted by the classical plasticity laws of isotropic or kinematic hardening (with Jaumann stress rate). Lipkin and Lowe[14] used a polycrystal model to produce this type of qualitative behavior although the match with experiment was not good. They also observed a slight amount of contraction at the center of the gauge section which was measured post mortem. They attributed it as due to buckling during the reverse straining.

These interesting results of Lipkin and Lowe serve as a major impetus for this current work. The question of whether the axial stress measured after strain reversal is really indicative of material response to simple shear or whether it is due to residual stress in the specimen after forward straining needs to be investigated. In other words, is the thin-walled specimen suitable for revese straining tests?

13

Also, it was desired to see if other materials showed the same interesting behavior seen in 304L stainless steel. This axial stress behavior is not predicted by the classical plasticity laws and it was desired to see what elements of a phenomenological constitutive theory could give this type of behavior. The program that addressed these concerns is outlined below.

First, the use of the thin-walled torsion specimen in reverse twist was investigated using the finite element model described above. The objective was to see whether the macroscopic stress strain response from the model was the same as the governing equations would give for simple shear or whether the experimental response derives from some special specimen response. Second, reverse torsion experiments were conducted using the thin-walled specimens of 316 stainless steel and 1100-O aluminum. These materials were chosen since a detailed data base has already been generated for them under a number of deformation modes including torsion (see White, Bronkhorst and Anand[9]). Finally, these reverse torsion tests were modeled using a number of the constitutive laws presented in the literature for modeling simple shear. Mainly, these included differing forms for the stress rate applied to Prager-Ziegler kinematic hardening.

FINITE ELEMENT RESULTS FOR REVERSE TWISTING

A finite element study was undertaken to investigate the suitability of using the thin-walled torsion specimen in reverse shear. This study was an extension of a detailed analysis of the torsion specimen discussed above. The same mesh and procedures described above were also used in this study. A single strip of 8 node, three dimensional brick elements was employed along with suitable kinematic constraints to simulate a full 360 degree circumferential mesh. The strip model had 8 elements along the radial direction and 44 elements along the axial extent from the specimen symmetry plane to the end of the shoulders. There were 8 x 15 elements in the half gauge length.

The end of the shoulder region was constrained such that it could not move in the axial direction. This simulated a fixed grip end condition.Recall that it was shown that axial strain can still be produced in the gauge section due to the induced stresses pulling the center of the specimen toward the axis. This effect is small and has been quantified.

The material model in this finite element simulation was linear kinematic hardening using the Jaumann derivative. An initial yield stress of 250 MPa and a constant plastic hardening modulus of 1500 MPa were used. These were chosen as an approximation to the compression test of 316 stainless steel reported in White, Bronkhorst and Anand although linear kinematic hardening would not give a good match to experiment for a uniaxial reverse test. A Young's modulus of 200 GPa and a Poisson's ratio of 0.33 were used for the elastic properties.

The model of the half specimen was twisted through an angle of 0.3 radians then the direction of twist was reversed and the specimen was twisted back to the original orientation. The reaction forces that were required were summed to give the torque and axial force. These reactions are analogous to the

14

values that would be measured by a load cell in an experiment. The macroscopic specimen stress response was determined using the thin-wall approximation by dividing the force by the initial cross sectional area and the torque by the area and mean radius. The average gauge shear strain was computed by assuming that a torsional extensometer could measure the twist across the gauge section and dividing by the gauge length.

The macroscopic stress response for this model is shown in Figure 9. The applied twist produced a maximum shear strain in the gauge section of 75%. The shear stress shows the type of response that is expected for a stress reversal with kinematic hardening. Notice that the strain magnitude is not large enough to show the stress oscillations that the Jaumann stress rate would produce. The normal stress response shows the development of a compressive axial stress during forward twisting and the interesting result that during reversal of the twist the stress subsides at almost exactly the same rate that it had developed. For linear hardening, the normal stress just increases and decreases along essentially the same curve. The finite element results essentially fall on top of predictions where the same material law was integrated using perfect simple shear deformation. This demonstrates the usefulness of the torsion specimen for simulating simple shear under these circumstances. Immediately it is obvious that the shape of the stress response curves are very different than those observed in the experiment of Lipkin and Lowe.[14] The use of the normal stress during reverse shear might be a good test for discriminating material models. This leads to the need to investigate the shape of the normal stress response during reversal of shear from both experimental and constitutive modeling viewpoints.
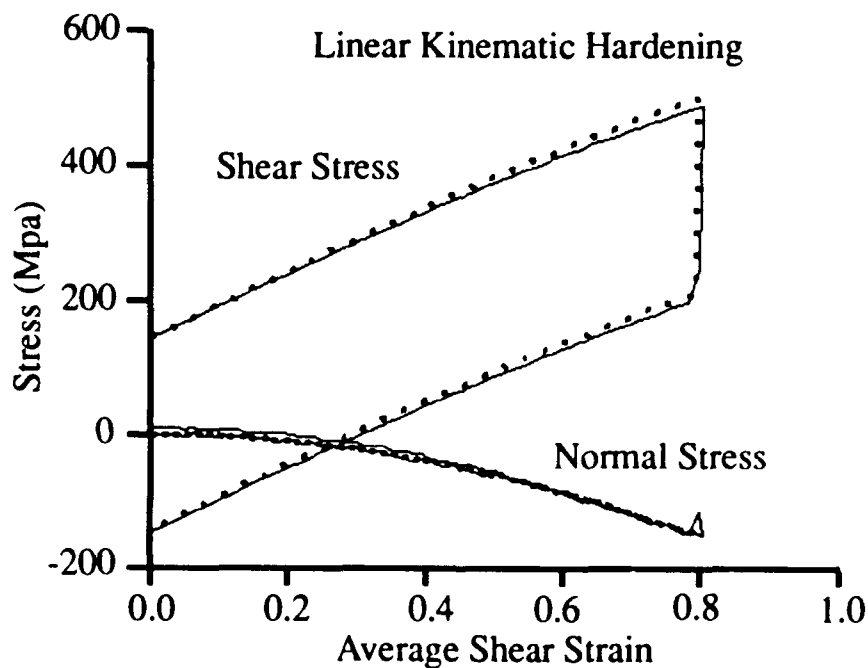

Figure 9. Finite element results for reverse torsion. Solid curve
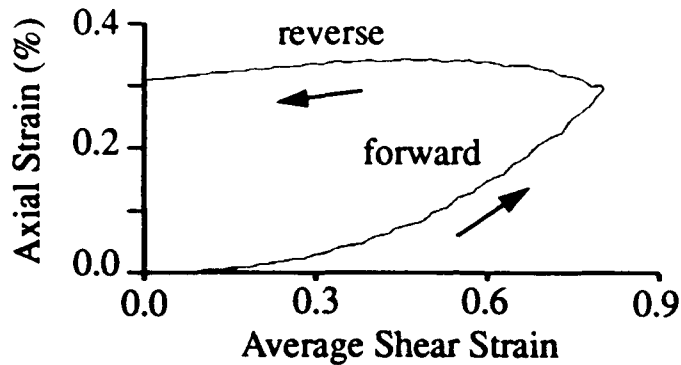iis finite element, dashed curve is simple shear integration.

Figure 10. Axial strain development during reverse twist.

One last observation can be made from the finite element analysis. The small amount of axial strain that accumulates during forward twist does not recover during reverse twist. Figure 10 shows the average axial strain across the gauge section as a function of the average shear strain. Notice that the axial strain remains fairly constant during the reverse twist portion of the curve.

REVERSE TORSION EXPERIMENTS

Reverse torsion experiments were conducted on thin-walled specimens having short gauge sections and thick shoulder regions. The specimen geometries and testing procedures are similar to those described in White et. al.[9] The inner bore of the shoulder region is fitted with a matched machined steel plug and the outer surface of the shoulder is gripped with an hydaulic collet type grip. This firmly holds the specimen and allows both axial and torsional forces to be applied with no backlash. The grips are controlled so that they experience no axial motion during the twisting to within the stiffness of the test frame. A constant twist rate is applied in one direction up until maximum rotation is reached, then the twist rate is reversed and the specimen twisted back to its original orientation. The twist rate was chosen so that the nominal equivalent strain rate in the gauge section was 0.001 mm/mm/sec. No separate measurement was made of the strain in the gauge section apart of what could be inferred from thegrip rotation and corrected for with the finite element correction. The stress and strain results were reduced from the raw data in the common way for thin-walled specimens as done above.

The results for the two experiments are given in Figure 11. The shear stress shows behavior very similar to reverse loading of a uniaxial specimen: plastic flow in the forward direction, elastic unloading, a reduced yield stress level during reversing, a smooth elastic-plastic transition, and fully developed plastic flow in the reverse direction. The axial stress response of 316 stainless steel in Figure 11a shows behavior similar, but not identical, to the results of Lipkin and Lowe.[14] During forward loading, the axial normal stress magnitude monotonically increases to 100 Mpa. This agrees with the magnitude reached in the torsion tests reported in White et. al.[9] During reverse loading, the stress magnitude quickly reduces to zero and then begins to increase compressively again. It reaches almost the same magnitude that it had prior to unloading by the time that the specimen is completely untwisted. The results for the 1100-O aluminum are similar to the 316 stainless steel but the shear stress shows a region of lower

16

strain hardening during the reversal. This behavor has been observed in uniaxial reverse flow for FCC materials that harden by subgrain formation. This is believed to be the first result that shows this behavior at strains this large. The axial normal stress development for the aluminum is similar in shape to that for stainless steel except that it shows a little initial peak during forward loading. This could be due to an inital anisotropy in the aluminum. Both materials were chosen and annealed to try to obtain as random an initial crystal orientation as possible but this may not have been perfect. No X-ray measurements have yet been made of the crystal structure either before or after deformation. Note that the
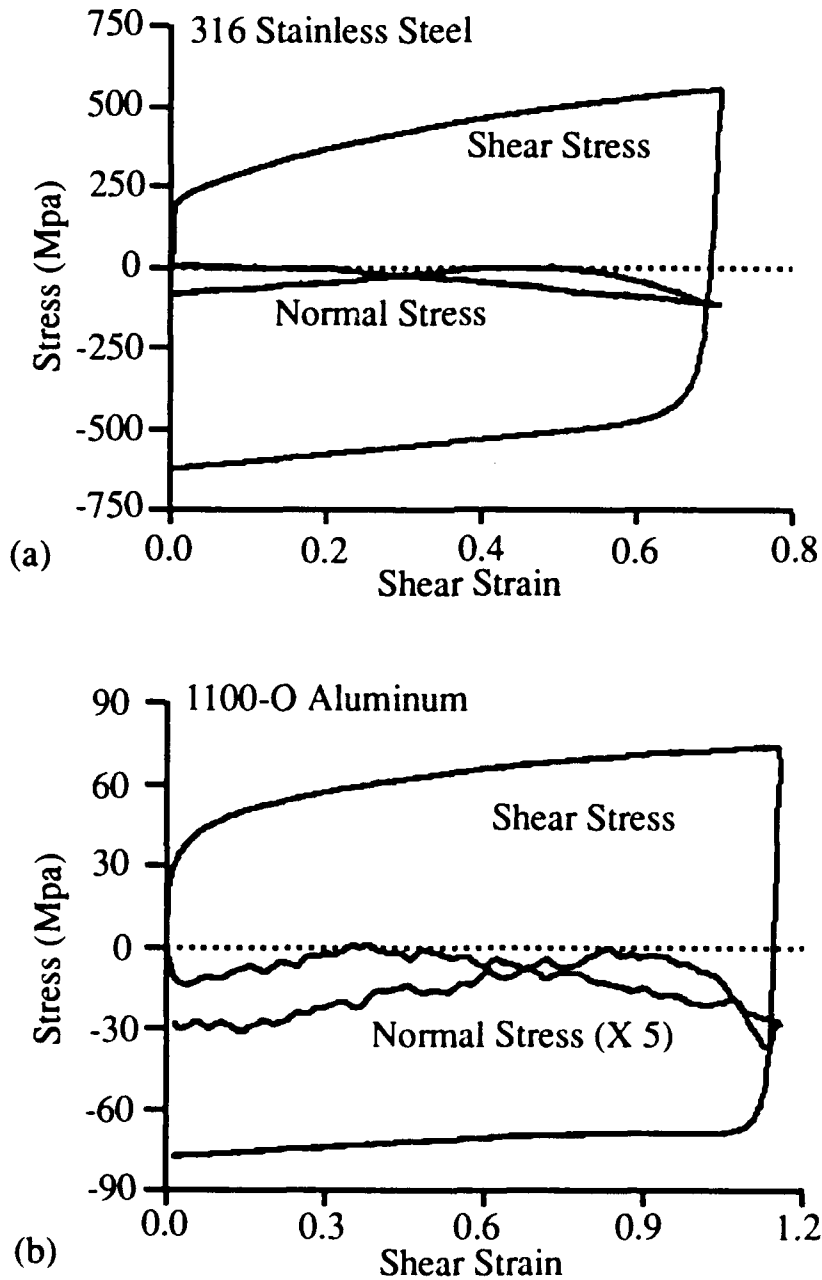

Figure 11. Reverse torsion test results.

normal stress for the aluminum has been multiplied by a factor of 5 so that it can appear on the same graph as the shear stress. The noise in the load stress response can be seen since the load signal was so small for the aluminum.

Detailed measurements of the geometry of the gauge section were not made during or after the test. Some surface roughening was observed in the gauge section as expected for plastic strains of these magnitudes. This was more pronounced in the aluminum than in the stainless steel.

PREDICTIONS OF REVERSE SHEAR WITH VARIOUS MODELS

The finite element results presented above show that classical Prager-Ziegler kinematic hardening using the Jaumann stress rate does not predict the observed axial normal stress reponse in reverse torsion. Many constitutive formulations have been proposed during the past decade which modifiy this constitutive law to remove the unwanted stress oscillations and match the axial stress seen in experiment. Among these proposals are: the use of the Green-Naghdi stress rate,[22] and the formulation of plastic spin in either phenomenological[23, 24] or micromechanical[25] frameworks. The reader is referred to these papers for details of the formulations and other references on the topic.

In this section, calculations using Jaumann, Green-Naghdi, and plastic spin motivated stress rates applied to kinematic hardening in simple shear are compared with the experimental results. Rigid-plastic simple shear calculations are used instead of full finite element simulations of the test specimen. These were much easier to calculate and modifiy than the FEM calculations would have been. It is shown above that simple shear is an adequate approximation to the macroscopic stress strain results derived from these test specimens. The plastic hardening modulus used in these calculations is derived from the compression test of 316 stainless steel. Here, the modulus is written as a function of accumulated plastic strain and is fit to the compression test data.

The first prediction of theory with experiment is shown in Figure 12. Here the Prager-Ziegler kinematic theory using the Jaumann stress rate is compared to the reverse torsion of 316 stainless steel. Notice that during forward twisting both the shear stress and the axial normal stress are predicted quite well by the theory. During the reverse twist portion of the results we see large discrepancies with the experiment. The shear stress does not unload to zero before fully developed plastic flow is predicted in the reverse direction. This is to be expected from any kinematic hardening theory having the Prager-Ziegler type evolution law for the back stress. The axial normal stress is predicted to monotonically increase in

22. Dienes, J.K., *On the Analysis of Rotation and Stress Rate in Deforming Bodies*, Acta Mechanica, Vol. 32, 1979, pp. 217-232.
23. Dafalias, Y.F., *The Plastic Spin comcept and a Simple Illustration of its Role in Finite Plastic Transformations*, Mechanics of Materials, Vol. 3, 1984, pp. 223.
24. Paulun, J.E., and Pecherski, R.B., *Study of Corotational Rates for Kinematic Hardening in Finite Deformation Plasticity*, Archives of Mechanics, Vol. 37, 1985, pp. 661-677.
25. Bammann, D.J., and Aifantis, E.C., *A Model for Finite-Deformation Plasticity*, Acta Mechanica, Vol. 69, 1987, pp. 97-117.

compressive magnitude during forward straining and to almost follow the loading curve during unloading. This is just the type of behavior shown in Figure 9. That is to be expected since Figure 9 shows Prager-Ziegler predictions for torsion of the specimen using the Jaumann stress rate. Again we note that this unloading prediction does not even qualitatively represent the experiment. It is interesting to note that for the stainless steel, the compressive stress that develops during finite twisting is well predicted with the Jaumann stress rate. At the strain level considered here the question of oscillatory stresses is not a problem.

Since the Jaumann stress rate does not exhibit the observed behavior during twist reversal the question arises as to whether any of the other proposed stress rates do any better. In Figure 13 are shown the normal stress predictions for reverse simple shear of Prager-Ziegler kinematic hardening using: the Green-Naghdi stress rate,[22] and the elastic spin type rates derived from the plastic spin formulations of Dafalias[23] and Paulun and Pecherski.[24] Of these objective stress rate theories only that due to Dafalias has an adjustable parameter once the plastic modulus is set. The reader is referred to the above cited papers for the details of the derivations. Here, just the results using them to simulate reverse simple shear are shown. Notice that each of these models predicts the right order of magnitude for the normal stress as it develops during forward straining but none of them predicts the correct behavior during reversal. Qualitatively they all give the same type of result as the predictions in Figure 12 using the Jaumann derivative..
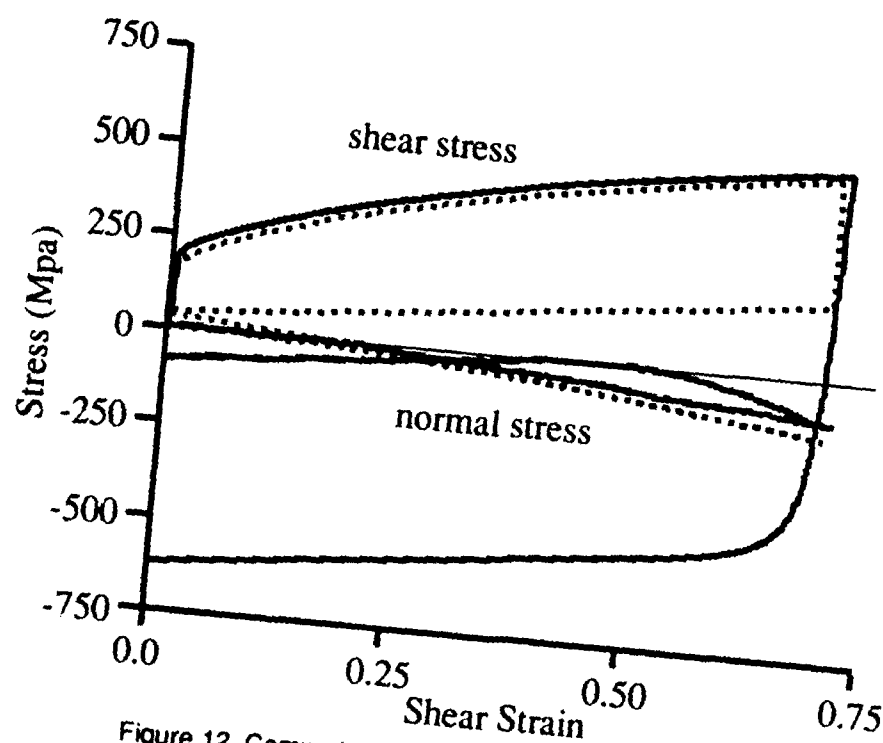

Figure 12. Comparison of stainless steel experiment with prediction of Jaumann stress rate kinematic hardening (solid curves are experiment, dashed curves are theory).
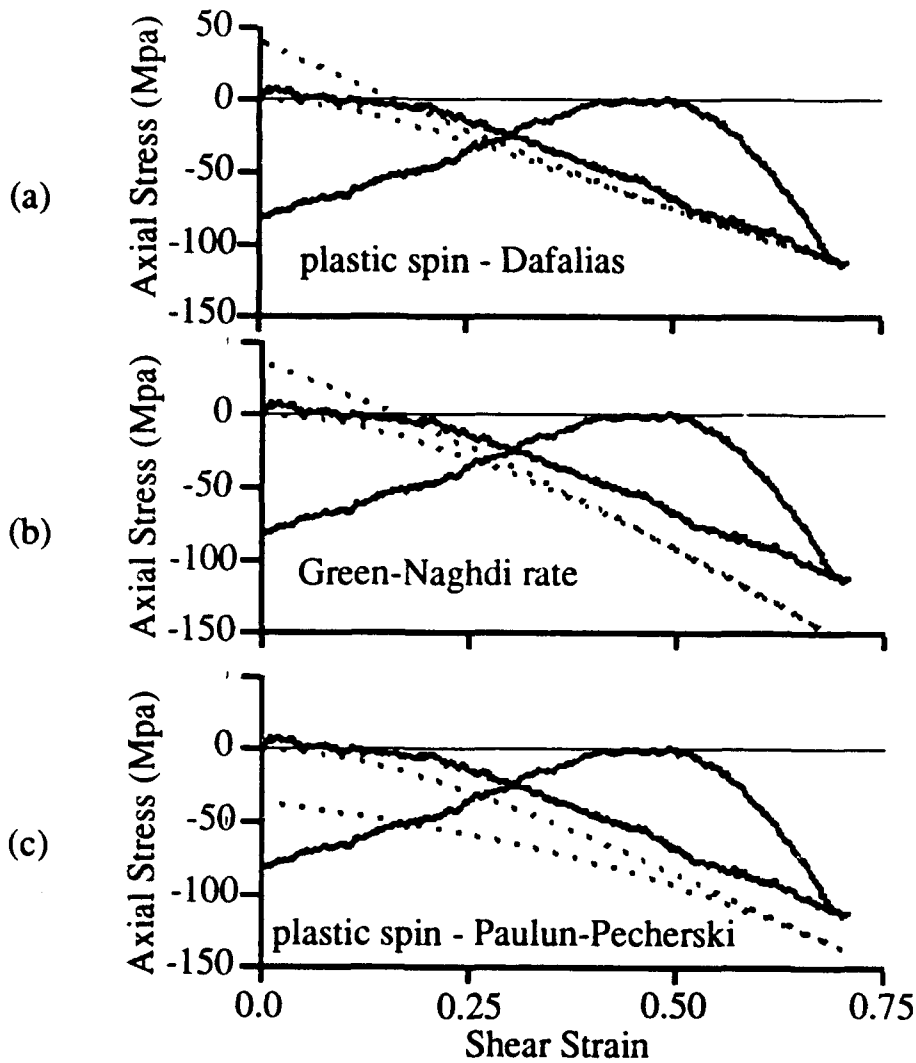
Figure 13. Axial normal stress predictions for various stress rates. Experiment is solid curve, theory is dashed.

All of the results presented above are for Prager-Ziegler kinematic hardening. It is natural to wonder what the results would be for an evanescent-type back stress evolution equation. This type of evolution law was used in White et al.[9] where the material constants were chosen from reverse loading experiments. It is important to remember that the additional evanscent term is used to model the elastic-plastic transition during reverse cycling. When realistic material constants are chosen in this way it was seen that the axial normal stress does not develop a large enough magnitude to model the experiments in forward loading. Some calculations have shown that evanescent hardening can produce a qualitatively better shape for the axial stress during reversal but the magnitude is an order of magnitude less than the experiments.

CONCLUSIONS

These results illustrate the usefulness of the reverse torsion test for evaluating material models. The results of the finite element model shows that the thin-walled torsion specimen gives the same macroscopic stress strain response in both forward and reverse twist as simple shear. The twist which the grips apply to the specimen goes partly into deforming the gauge section and partly into deforming the shoulder region. A correction factor has been determined for use in reducing the machine rotation into the gauge region shear strain. This factor was found to be independent of the material models considered here. The stress and strain variations within the gauge section were also quantified. The reverse torsion experiments give results that are qualitatively similar to those reported in Lipkin and Lowe.[14] The axial normal stress initially decreases to zero but then increases back to its value prior to unloading. This behavior is not predicted by Prager-Ziegler kinematic hardening using any of the corotational stress rates considered. Further research is warranted to investigate what phenomenological theories can reproduce this behavior without sacrificing the ability to model other phenomena such as uniaxial cyclic loading. The thin-walled torsion test provides a new and useful tool for modeling the deformation of metals.

No of Copies	To
1	Office of the Under Secretary of Defense for Research and Engineering, The Pentagon, Washington, DC 20301
1	U.S. Army Materiel Command, 5001 Eisenhower Avenue, Alexandria, VA 22333-0001 ATTN: AMCLD

Commander, U.S. Army Laboratory Command, 2800 Powder Mill Road, Adelphi, MD 20783-1145
| 1 | ATTN: AMSLC-IM-TL |
| 1 | AMSLC-CT |

Commander, Defense Technical Information Center, Cameron Station, Building 5, 5010 Duke Street, Alexandria, VA 22304-6145
| 2 | ATTN: DTIC-FDAC |

| 1 | Metals and Ceramics Information Center, Battelle Columbus Laboratories, 505 King Avenue, Columbus, OH 43201 |

Commander, Army Research Office, P.O. Box 12211, Research Triangle Park, NC 27709-2211
| 1 | ATTN: Information Processing Office |

Commander, U.S. Army Electronics Technology and Devices Laboratory, Fort Monmouth, NJ 07703-5000
| 1 | ATTN: SLCET-DT |

Commander, U.S. Army Missile Command, Redstone Arsenal, AL 35898-5247
| 1 | ATTN: AMSMI-RD-CS-R/DOC |
| 1 | AMSMI-RLM |

Commander, U.S. Army Armament, Munitions and Chemical Command, Dover, NJ 07801
| 2 | ATTN: SMCAR-TDC |

Commander, U.S. Army Natick Research, Development and Engineering Center, Natick, MA 01760-5010
| 1 | ATTN: Technical Library |

Commander, U.S. Army Tank-Automotive Command, Warren, MI 48397-5000
| 1 | ATTN: AMSTA-TSL, Technical Library |

Commander, U.S. Army Engineer Waterways Experiment Station, P.O. Box 631, Vicksburg, MS 39180
| 1 | ATTN: Research Center Library |

Director, U.S. Army Ballistic Research Laboratory, Aberdeen Proving Ground, MD 21005
1	ATTN: SLCBR-DD-T (STINFO)
1	SLCBR, Dr. J. Huffington
1	SLCBR, Dr. J. Walter
1	SLCBR, Dr. Thomas W. Wright

Director, Benet Weapons Laboratory, LCWSL, USA AMCCOM, Watervliet, NY 12189
| 1 | ATTN: AMSMC-LCB-TL |

Commander, U.S. Army Foreign Science and Technology Center, 220 7th Street, N.E., Charlottesville, VA 22901-5396
| 1 | ATTN: AIAST-RA-ST |

Director, Eustis Directorate, U.S. Army Air Mobility Research and Development Laboratory, Fort Eustis, VA 23604-5577
| 1 | ATTN: SAVDL-E-MOS (AVSCOM) |

Director, Langley Directorate, U.S. Army Air Mobility Research and Development Laboratory, NASA-Langley Research Center, Hampton, VA 23665
| 1 | ATTN: Aerostructures Directorate |

Naval Research Laboratory, Washington, DC 20375
| 1 | ATTN: Code 5830 |

Office of Naval Research, 800 North Quincy Street, Arlington, VA 22217-5000
| 1 | ATTN: Mechanics Division, Code 1132-SM |
| 1 | Dr. Roshdy Barsoum |

No of Copies	To
	Naval Air Development Center, Warminster, PA 18974-5000
1	ATTN: Code 6064
1	AVCSTD/6043
	U.S. Navy David Taylor Research Center, Bethesda, MD 20084
1	ATTN: Code 172
	U.S. Air Force Office of Scientific Research, Bolling Air Force Base, Washington, DC 20332
1	ATTN: Mechanics Division
	Commander, U.S. Air Force Materials Laboratory, Wright-Patterson Air Force Base, OH 45433
1	ATTN: AFWAL/MLLN
	National Aeronautics and Space Administration, Marshall Space Flight Center, Huntsville, AL 35812
1	ATTN: EH01, Dir, M&P Lab
1	Committee on Marine Structures, Marine Board, National Research Council, 2101 Constitution Avenue, N.W., Washington, DC 20418
	Director, U.S. Army Materials Technology Laboratory, Watertown, MA 02172-0001
2	ATTN: SLCMT-TML
1	Author